Coplanar structures in $L=0$ even-parity intrashell states of four-valence-electron atoms

Bao Chengguang
China Center of Advanced Science and Technology (World Laboratory), P.O. Box 8730, Beijing 100080, China and Department of Physics, Zhongshan University, Guangzhou, China

Duan Yiwu
Department of Physics, Hunan Normal University, Changsha, Hunan Province, China

(Received 18 February 1993)

A model with all radial degrees of freedom frozen is used to simulate the $^{2S+1}S^e$ intrashell states of four-valence-electron atoms. By inspecting the two-body densities, the latitudinal distribution functions, and by inspecting directly the eigenfunctions in appropriate subspaces, the features of geometric structure and of internal motion have been obtained. The effect of the spatial permutation symmetry and the parity have been emphasized. All even-parity states under consideration prefer the coplanar axial-symmetric structure. Two modes of motion are found, namely, the triple two-body collision mode and the rectangle-square-rectangle mode (or planar double two-body collision mode). It is found that the basic modes in quantum states are associated with periodic solutions of classical mechanics.

PACS number(s): 31.50.+w, 03.65.Ge, 31.20.Tz, 31.20.Di

I. INTRODUCTION AND THE PROCEDURE

In a previous work [1] the odd-parity $L=0$ intrashell states of an atomic system with four (valence) electrons have been investigated within an r-frozen model (all r_i are given at an optimal value). This paper is a continuation to investigate the even-parity states. The background and the motivation are referred to in [1] and for related references the reader is referred to [2–5]. The same model and a similar procedure of analysis are used. In brief, the Hamiltonian

$$H=\frac{\hbar^2}{2mr_0^2}\sum_{i=1}^{4}\hat{l}_i^2+\sum_{\substack{i,j\\ i<j}}\frac{e^2}{|\mathbf{r}_i-\mathbf{r}_j|} \tag{1}$$

is diagonalized in a model space spanned by antisymmetrized basis functions

$$\tilde{\Phi}_i=\mathcal{A}(\{[Y_{l_1}(\hat{1})Y_{l_2}(\hat{2})]_{l_{12}}[Y_{l_3}(\hat{3})Y_{l_4}(\hat{4})]_{l_{34}}\}_L \times\chi^{M_S}_{s_1s_2S}(1234)) . \tag{2}$$

The labels are the same as in [1]. $\mathbf{r}_i\equiv r_0\hat{\mathbf{r}}_i$ originates from the nucleus at the origin and r_0 is fixed for all four electrons; $\hat{\mathbf{r}}_i$ is written in short as $\hat{i}$ in Eq. (2). In order to have the results comparable with those of [1], the same value of $r_0=0.62$ Å is assumed. The spins of electrons e_1 and e_2 are coupled to s_1, those of e_3 and e_4 are coupled to s_2, s_1 and s_2 are coupled to S, and the Z component of S is M_S. The number of basis functions are restricted by the constraint $0\le l_i\le l_{\max}$, where $i=1$, 2, 3, or 4. Since we are interested only in the qualitative aspect, and since we are mostly interested in the head states (the lowest state of a given $^{2S+1}L^{\pi}$ symmetry), $l_{\max}$ is given as 2. This choice is found to be sufficient for our purpose.

Though the interactions are spin independent, the e-e correlations are strongly spin dependent [6]; this is a striking feature of fermion systems. Hence, if we insist on carrying out a spin-independent analysis, our results would be unclear. Since we are interested in the fine features of e-e correlation, a spin-dependent analysis is absolutely necessary. There may be different choices. In the first choice the eigenfunction

$$\Psi=\sum_i c_i\tilde{\Phi}_i \tag{3}$$

is expanded as

$$\Psi=\sum_{s_1,s_2}F_{s_1s_2}(\hat{1}\hat{2}\hat{3}\hat{4})\chi^{M_S}_{s_1s_2S}(1234) . \tag{4}$$

Then each $F_{s_1s_2}(\hat{1}\hat{2}\hat{3}\hat{4})$ component is subjected to analysis; accordingly the information extracted is s_1 and s_2 dependent. In the second choice Ψ is expanded as

$$\Psi=\sum_{\mu_1,\mu_2,\mu_3}f_{\mu_1\mu_2\mu_3\mu_4}(\hat{1}\hat{2}\hat{3}\hat{4})\xi_{\mu_1}(1)\xi_{\mu_2}(2)\xi_{\mu_3}(3)\xi_{\mu_4}(4) \quad(\mu_4=M_S-\mu_1-\mu_2-\mu_3) . \tag{5}$$

Then each $f_{\mu_1\mu_2\mu_3\mu_4}(\hat{1}\hat{2}\hat{3}\hat{4})$ component is subjected to analysis; accordingly the information extracted is μ_1,μ_2,μ_3 and M_S dependent. From the antisymmetrization of Ψ we have

$$f_{\mu_1\mu_2\mu_3\mu_4}(\hat{1}\hat{2}\hat{3}\hat{4})=(-1)^p f_{\mu_{p_1}\mu_{p_2}\mu_{p_3}\mu_{p_4}}(\hat{p}_1\hat{p}_2\hat{p}_3\hat{p}_4) , \tag{6}$$

where $p_1p_2p_3p_4$ is any permutation of 1234. This symmetry would facilitate the analysis (among all $f_{\mu_{p_1}\mu_{p_2}\mu_{p_3}\mu_{p_4}}$ components with different $p_1p_2p_3p_4$, the analysis of only one component is sufficient). In what follows, the second choice is adopted; it implies that the polarity of each electron is specified during the analysis (ac-

cordingly, it implies that the polarity is assumed to be experimentally measurable).

There are three cases, i.e., $S=0$, 1, or 2. In order to have the same polarity for these three cases such that their results can be compared with each other, $M_S=0$ is assumed. This implies that we have two spin-up (in short, up) electrons and two down electrons. Once M_S is given, the last subscript in $f_{\mu_1\mu_2\mu_3\mu_4}$ may be neglected. Thus it is often simply denoted as $f_{\mu_1\mu_2\mu_3}$. With this prescription, we have the spin-parallel two-body density

$$\rho_{\uparrow\uparrow}(\mathcal{R}\theta_{12})=\frac{8\pi^2}{2L+1}\sum_{\mu_1,\mu_2,\mu_3}\delta_{\mu_1\mu_2}\int d\hat{r}_3 d\hat{r}_4 |f_{\mu_1\mu_2\mu_3}|^2 , \tag{7a}$$

where $\mathcal{R}$ labels the orientation of a body frame fixed at the plane of $\mathbf{r}_1$ and $\mathbf{r}_2$ (states of $L=0$ are $\mathcal{R}$ irrelevant), θ_{12} is the angle between $\mathbf{r}_1$ and $\mathbf{r}_2$, and the spin-antiparallel two-body density

$$\rho_{\uparrow\downarrow}(\mathcal{R}\theta_{12})=\frac{8\pi^2}{2L+1}\sum_{\mu_1,\mu_2,\mu_3}(1-\delta_{\mu_1\mu_2})\int d\hat{r}_3 d\hat{r}_4 |f_{\mu_1\mu_2\mu_3}|^2 . \tag{7b}$$

They can be weighted as

$$\tilde{\rho}_{\uparrow\uparrow}=\rho_{\uparrow\uparrow}\sin\theta_{12} , \quad \tilde{\rho}_{\uparrow\downarrow}=\rho_{\uparrow\downarrow}\sin\theta_{12} . \tag{8}$$

The usual two-body density is the sum of Eqs. (8)

$$\rho_2=\rho_{\uparrow\uparrow}+\rho_{\uparrow\downarrow} , \quad \tilde{\rho}_2=\tilde{\rho}_{\uparrow\uparrow}+\tilde{\rho}_{\uparrow\downarrow} . \tag{9}$$

The above quantities together with a latitudinal distribution function (defined later) and with the $f_{\mu_1\mu_2\mu_3}$ itself will be presented.

Incidentally, the integration involved in all the above correlation (distribution) functions can be carried out analytically (refer to the Appendix of [1]) to facilitate numerical calculation.

II. ENERGY SPECTRUM

In what follows in general only the results of $l_{\max}=2$ are reported. The energy spectrum is given in Fig. 1. It shows that the energy of the $^1S^e$ head state is only slightly higher than the $^5S^o$ head state (this situation is similar to three-electron intrashell states, where the energies of the $^2S^e$ and $^4S^o$ head states are very close). It is recalled that the $^5S^o$ head state has the most favorable equilateral tetrahedron (ETH) structure [1]. In this configuration a space inversion, together with an interchange of the positions of any pair of particles, is equivalent to an appropriate spatial rotation. In $L=0$ even states, this implies that the ETH is only available if the spatial part of the wave functions is all symmetric. Evidently this is not possible for all $^{2S+1}S^e$ states, simply because the spin part cannot be all antisymmetrized. Hence the low energy of the $^1S^e$ head state surely implies that another favorable geometric structure exists.

Figure 1 shows that there are a number of low-lying angularly excited $^1S^e$ states. On the contrary, in the $^5S^o$ states, there is a large gap lying between the head state and the first excited state. Hence the $^1S^e$ head state is much more easily excited than the $^5S^o$ head state with respect to symmetry-conserving angular excitation (L,S, parity, and the principle quantum numbers are conserved).

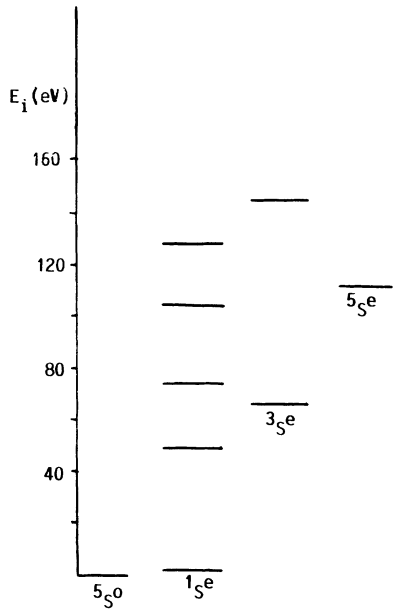

FIG. 1. Energy spectrum (in eV) of the $^{2S+1}S^e$ states with $r_0=0.62$ Å and $l_{\max}=2$. The energy of the $^5S^o$ head state is scaled as zero.

Among the six $^{2S+1}S^\pi$ head states ($S=0$, 1, or 2 and π is even or odd), the $^5S^e$ head state has a particular high energy while the $^5S^o$ head state is the lowest. This fact alone implies a decisive effect of parity on structures. The physics underlying the spectrum will be discussed later.

III. COPLANAR STRUCTURES

A striking feature found in all the $^{2S+1}S^e$ states (head or excited) is the preference of coplanar structure, i.e., all four electrons together with the core prefer to stay in a plane. Let us first consider this point from symmetry. Hereafter, let the spins of e_1 and e_2 be up and, accordingly, e_3 and e_4 down (the choice of any pair of electrons to be up is irrelevant). Let the plane formed by e_1, e_2 and the core be denoted as Σ. If the five particles do not stay in a plane, e_3 and e_4 may "look" for a three-dimensional configuration having a better geometric structure to have a stronger binding (weaker repulsion). A good candidate will have e_3 and e_4 separated by the two sides of Σ and symmetric to this plane (the ETH is a special case of this candidate). However, in this candidate a space inversion, together with a 180° spatial rotation in Σ, is equivalent to an interchange of e_3 and e_4; the former operation has no effect while the latter operation causes a reversal of sign in the wave function. Hence this candidate is prohibited by the quantum-mechanical (QM) symmetry. It implies that if the $^{2S+1}S^e$ states looked for a three-dimensional structure, they could not find one having a better

geometric symmetry. This may be the background of the preference of the coplanar structures.

Now let us confirm this preference by inspecting the eigenfunctions. Let the above Σ plane be denoted as the X-Y plane (where the nucleus is at the origin) and let us ignore the position of e_4 and ignore the longitudinal distributions of e_1, e_2, and e_3, but observe only the latitudinal distribution of e_3. For this purpose we define the latitudinal distribution function

$$P_{\mu_1\mu_2\mu_3}(\theta_1\theta_2\theta_3)=\sin\theta_1\sin\theta_2\sin\theta_3 \times \int d\phi_1 d\phi_2 d\phi_3 d\hat{r}_4 |f_{\mu_1\mu_2\mu_3}|^2 . \quad (10)$$

When $\theta_1=\theta_2=90°$, $P_{\frac{1}{2}\frac{1}{2}\frac{\uparrow}{2}}$ as functions of θ_3 are plotted in Fig. 2(a) for the $^1S^e$ state and in Fig. 2(b) for the $^1S^o$ state for comparison. The preference of being coplanar is explicitly shown in Fig. 2(a), where the distribution is around $\theta_3=90°$. If we ignore e_3 but observe e_4, we obtain exactly the same result simply because of the antisymmetrization. On the other hand, the distribution in Fig. 2(b) is explicitly lying away from $\theta_3=90°$. It was found that the $P_{\frac{1}{2}\frac{1}{2}\frac{\uparrow}{2}}$ of the $^3S^e$ and the $^5S^e$ states are very similar to the $^1S^e$ state, while those of the $^3S^o$ and the $^5S^o$ states are very similar to the $^1S^o$ state. Thus the structures of the even and odd states should be greatly different.

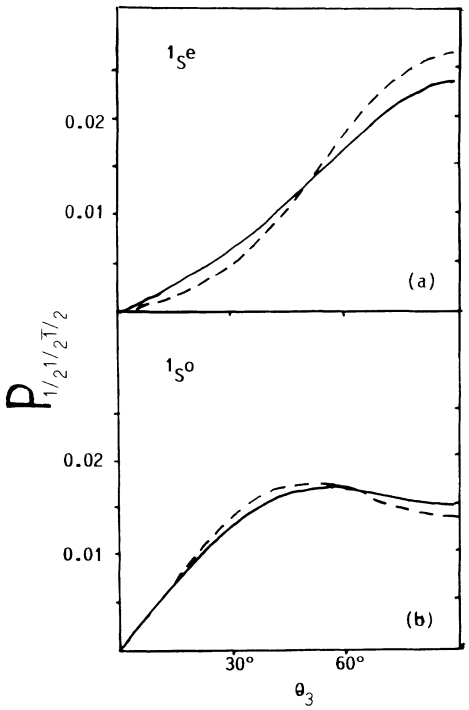

FIG. 2. The latitudinal distribution functions $P_{\frac{1}{2}\frac{1}{2}\frac{\uparrow}{2}}$ as a function of θ_3, $\theta_1=\theta_2=90°$ is assumed. The solid curve is for the head state and the dashed curve is for the first excited state.

IV. AXIAL SYMMETRY

Making use of the findings of Sec. III, we shall confine our observation in the subspace $\theta_i=90°$ $(i=1-4)$ to simplify the analysis further. Let us define the X-Y plane as before and choose the X axis such that $\phi_1=-\phi_2$. Then let us fix ϕ_1 at a number of values, in every case $f_{\frac{1}{2}\frac{1}{2}\frac{\uparrow}{2}}$ of the $^3S^e$ head state, as functions of ϕ_3 and ϕ_4 are plotted in contour diagrams. Three of them are representatives as shown in Figs. 3(a)–3(c). From Fig. 3(b) one may suggest two kinds of internal motion: one is associated with the distribution along PQ, the other one associated with $P'Q'$. There are nodes in the former, thus it implies an energetic motion when the system evolves along PQ. There is no node in the latter, thus it implies a weak motion when the system evolves along $P'Q'$. Evidently, the former is more important. In fact, the latter can be considered as only a small oscillation coupled to the main mode.

In the main mode, every pair of spin-parallel electrons (e_1 and e_2, and e_3 and e_4) keep the symmetry with respect to the X axis (thus it is a common axis of symmetry). When ϕ_1 changes, the patterns of corresponding figures also changes. This implies that the motion of the (e_1e_2) pair is coupled with the (e_3e_4) pair. This correlated motion is called an axial-symmetric mode. Accordingly, the small oscillation along $P'Q'$ is called an asymmetric motion. It turns out that the axial-symmetric motion as an important mode is generally established in all $^{2S+1}S^e$ states. In what follows we shall neglect the less important asymmetric motion to simplify the analysis. Only the results of the head states of specified symmetry will be reported.

V. $^1S^e$ HEAD STATE

We remind the reader that there are two up electrons and two down electrons. The two-body densities are shown in Figs. 4(a) and 4(a'). It shows that the feature of $\rho_{\uparrow\uparrow}$ is very different from $\rho_{\uparrow\downarrow}$, hence the correlation is strongly spin-polarity dependent. In particular, the spin-antiparallel pair has a much larger probability to have the two electrons closer. These figures are similar to Fig. 9 of [7] obtained from a two-shell model, where the radial degrees of freedom are not frozen but are still constrained by the model space. Incidentally, the limitation on $l_{\max}$ adopted in our model reduces the effects of e-e repulsion; it is no longer infinite at zero separation. If this limitation is removed, the overlap of two electrons is not possible and all the two-body densities should be zero at $\theta_{12}=0°$.

In order to observe the axial-symmetric motion, let $\theta_1=\theta_2=\theta_3=\theta_4=90°$, $\phi_1=-\phi_2$, and $\phi_3=-\phi_4$; then $f_{\frac{1}{2}\frac{1}{2}\frac{\uparrow}{2}}$ as a function of ϕ_1 and ϕ_3 is given in Fig. 5(a). There are two peaks A and B, both associated with a rectangle intuitively shown in Fig. 6. In this rectangle each longer side has a spin-parallel pair at its two ends with an angular separation 104°, this is associated with the peak of $\tilde{\rho}_{\uparrow\uparrow}$ in Fig. 4(a'). Each shorter side has a spin-antiparallel pair at its two ends and each diagonal has

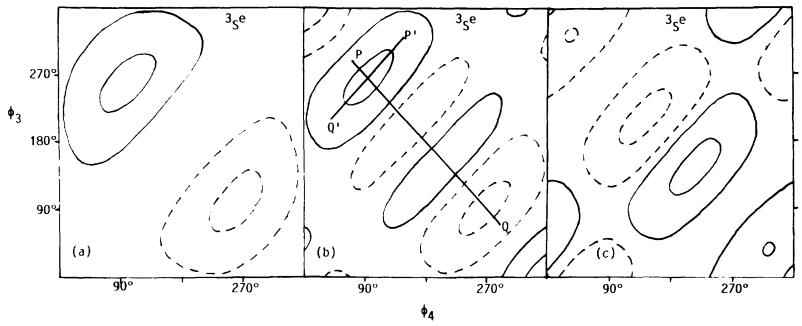

FIG. 3. $f_{\frac{1}{2}\frac{1}{2}\frac{1}{2}}$ as functions of ϕ_3 and ϕ_4 of the $^3S^e$ head state (real part only, the imaginary part is zero). $\theta_1=\theta_2=\theta_3=\theta_4=90°$ is assumed; $\phi_1=-\phi_2$ is given at 20°, 50°, and 80° in (a), (b), and (c), respectively. The contours of the positive values are represented by the solid line, the negative values are shown by the dashed line. They give ±84% or ±20% of the maximum.

also a spin-antiparallel pair at its two ends; this explains that there are two peaks in $\tilde{\rho}_{\uparrow\downarrow}$ in Fig. 4(a').

One may ask why the most probable configuration is a rectangle rather than a square. This arises because the correlation between the spin-parallel pair and that between the spin-antiparallel pair are different; the electrons can be closer in the latter case. One may ask why it is the spin-antiparallel pair rather than the spin-parallel pair that stays at the two ends of the diagonal. We remind the reader that an interchange of two spin-parallel electrons results in a reversal of sign in the wave function. If the latter case held, the square configuration would associate with a node simply because an interchange of the electrons at the two ends of a diagonal is equivalent to a 180° rotation about the other diagonal. However, a head state would not prefer to have a node close to its most probable shape (if it did, the kinetic energy would increase). This explains why the spin-parallel electrons do not stay at the two ends of a diagonal.

From the smooth distribution the internal motion of this state is recognized as a small oscillation around the rectangle. Although this state does not have as much of a favorable ETH configuration as the $^5S^o$ head state does, there is no node involved in the internal motion while the $^5S^o$ has one. This explains why the $^1S^e$ head state has an energy close to the $^5S^o$ head state.

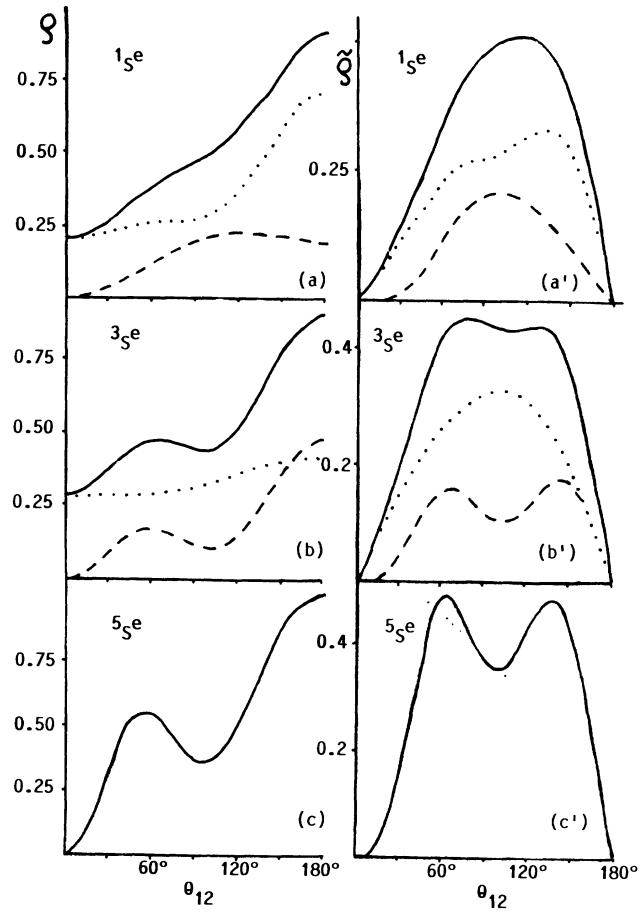

FIG. 4. Two-body densities. On the left-hand side the dashed line is for $\rho_{\uparrow\uparrow}$, the dotted line is for $\rho_{\uparrow\downarrow}$, and the solid line is for ρ_2. In (c), since $\rho_{\uparrow\uparrow}=\frac{1}{2}\rho_{\uparrow\downarrow}$, only ρ_2 is plotted. Corresponding weighted densities are on the right-hand side.

VI. $^3S^e$ HEAD STATE

It is recalled that the frame is so chosen that there are two up electrons e_1 and e_2 and two down electrons e_3 and e_4. The two-body densities are plotted in Figs. 4(b) and 4(b'). There are two peaks in $\tilde{\rho}_{\uparrow\uparrow}$; this is a noticeable feature. One may suggest that the interdistance of one spin-parallel pair is much longer (smaller) than that of the other spin-parallel pair. Taking into account the coplanar and axial-symmetric structure, the most probable shape is thus suggested as an isosceles trapezoid, as shown later.

Let us confine the observation in the same subspace of Fig. 5(a); then $f_{\frac{1}{2}\frac{1}{2}\frac{1}{2}}$ is given in Fig. 5(b). There are two maxima A and B and two minima C and D; each associates with a trapezoid. For example, the configuration as-

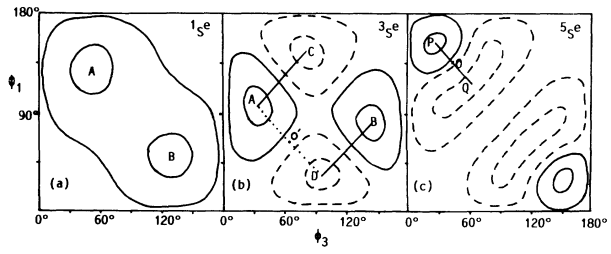

FIG. 5. $f_{\frac{1}{2}\frac{1}{2}\frac{1}{2}}$ as functions of ϕ_1 and ϕ_3. $\theta_1=\theta_2=\theta_3=\theta_4=90°$, $\phi_2=-\phi_1$, and $\phi_4=-\phi_3$ are assumed. Refer to the captions of Fig. 3.

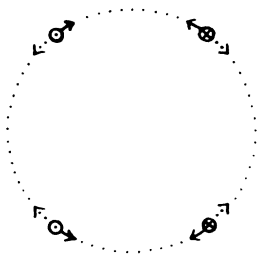

FIG. 6. The most probable shape of the $^1S^e$ head state, which is a rectangle lying in a plane containing the nucleus. The spin-up electron is marked by ⊙, spin-down by ⊗.

sociated with point A is plotted in Fig. 7(a) and that associated with C is in Fig. 7(b). Two types of motion can be suggested.

First, the system may evolve from A to C (crossing a nodal surface) as intuitively shown by the arrows in Fig. 7(a). When the system arrives at C, among six interelectronic distances three of them are small ($\theta_{ij} \leq 65°$). Hence three two-body collisions occur simultaneously, i.e., those between e_1 and e_2, e_1 and e_3, and e_2 and e_4; we call this a triple two-body collision (T2BC). Afterwards, the Coulomb repulsion pushes the electrons back to A to undergo the next T2BC at the other side of the nucleus. These successive collisions happen repeatedly, and it is called a planar T2BC mode. In this mode, mostly, e_1 and e_3 (correspondingly, e_2 and e_4) move along the same direction. The collective correlation is also shown in Fig. 3, where when ϕ_1 ($=-\phi_2$) increases from 20° to 80°, the location of the maximum becomes closer to $\phi_3=-\phi_4=180°$.

Second, the system may evolve from A to D by crossing another nodal surface; at the midpoint of AD e_l overlaps with e_3 and e_2 overlaps with e_4. However, this possibility is not realistic due to the infinite e-e repulsion at zero separation. Hence we shall ignore this possibility of motion. In fact, it was found that the larger the $l_{\max}$ adopted, the smoother the gradient of the wave function at O' [marked in Fig. 5(b)], thus the weaker the motion.

There is a nodal line appearing at $\phi_1=180°-\phi_3$ (a rectangle) in the T2BC mode. We shall show the origin of this line.

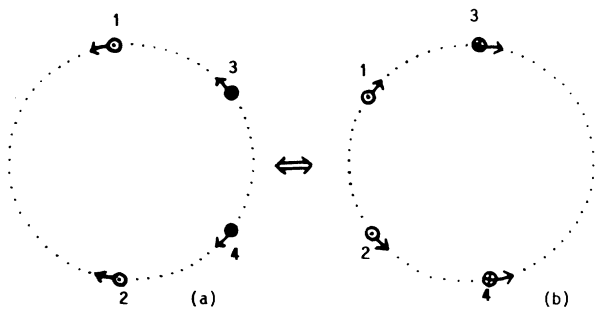

FIG. 7. The most probable shape of the $^3S^e$ head state which is an isosceles trapezoid; the planar T2BC mode is also intuitively shown by the arrows.

From Eq. (6), we have

$$f_{\mu_1\mu_2\mu_3\mu_4}(\hat{1}\hat{2}\hat{3}\hat{4})=f_{\mu_3\mu_4\mu_1\mu_2}(\hat{3}\hat{4}\hat{1}\hat{2}) . \tag{11}$$

From the definition, we have

$$f_{\mu_1\mu_2\mu_3\mu_4}(\hat{1}\hat{2}\hat{3}\hat{4})=\sum_{s_1,s_2} F_{s_1s_2}(\hat{1}\hat{2}\hat{3}\hat{4})C^{SM_S}_{s_1\mu_{12},s_2\mu_{34}} \times C^{s_1\mu_{12}}_{\frac{1}{2}\mu_1,\frac{1}{2}\mu_2} C^{s_2\mu_{34}}_{\frac{1}{2}\mu_3,\frac{1}{2}\mu_4}$$

$$=(-)^S f_{\bar{\mu}_1\bar{\mu}_2\bar{\mu}_3\bar{\mu}_4}(\hat{1}\hat{2}\hat{3}\hat{4}) . \tag{12}$$

Combining Eqs. (11) and (12), we have

$$f_{\frac{1}{2}\frac{1}{2}\bar{\frac{1}{2}}\bar{\frac{1}{2}}}(\hat{1}\hat{2}\hat{3}\hat{4})=(-)^S f_{\frac{1}{2}\frac{1}{2}\bar{\frac{1}{2}}\bar{\frac{1}{2}}}(\hat{3}\hat{4}\hat{1}\hat{2}) . \tag{13}$$

Equation (13) implies that, in our case, the interchange of the positions of an up electron with an adjacent down electron together with an interchange of the other two results in a reversal of sign in the wave function. On the other hand, if the particles form a rectangle, these simultaneous interchanges are equivalent to a 180° rotation, and thus should have no effect in $L=0$ states. For this reason, the rectangle is prohibited. Accordingly, the internal motion of the $S=1$ states are greatly different from the $S=$(even) states; this is a vivid example to show how the total spin affects the structure. Since there is a node involved in the motion of the $^3S^e$ head state but none in the $^1S^e$ head state, this explains why the former is higher.

VII. $^5S^e$ HEAD STATE

The two-body densities are shown in Fig. 4(c) and 4(c'). There are two peaks in $\tilde{\rho}_2=3\tilde{\rho}_{\uparrow\uparrow}=\frac{3}{2}\tilde{\rho}_{\uparrow\downarrow}$. In fact, in the $^5S^e$ states, the e-e spatial correlation is spin-polarity independent. Let us confine the observation in the same subspace of Fig. 5(a); then $f_{\frac{1}{2}\frac{1}{2}\bar{\frac{1}{2}}}$ is plotted in Fig. 5(c). The evolution along POQ implies a transformation from a flattened rectangle to a prolonged rectangle via a square; this is called an R-S-R mode. In this mode the square is associated with a node (marked by O), this node has a similar origin as we have discussed in Sec. V. (Notice that in the $^5S^e$ states an interchange of the positions of any pair of particles results definitely in a reversal of sign.)

When the rectangle is flattened, the two electrons at the two ends of a shorter side collide, as well as the other two electrons at the two ends of the other shorter side. This is also true when the rectangle becomes prolonged. Hence, during the R-S-R mode, double two-body collisions, as intuitively shown in Fig. 8, occur repeatedly and very rapidly. Since there is a nodal surface involved in this oscillation, it is no doubt an energetic mode.

VIII. FINAL REMARKS

We have used an r-frozen model to investigate the qualitative details of e-e correlation in $L=0$ even-parity

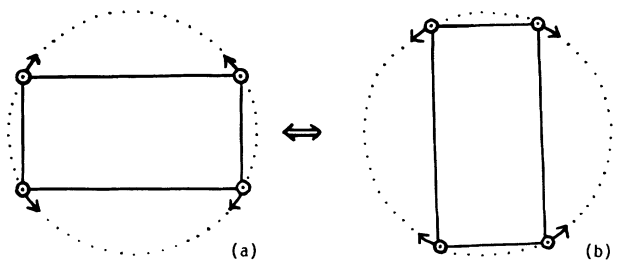

FIG. 8. Intuitive expression of the energetic R-S-R mode, where double two-body collisions occur very frequently.

intrashell states of 4-valence-electron atoms. The effect of the QM symmetry and the dynamical consequence of e-e correlation have been emphasized. Geometric features of the structures and modes of internal motion have been found. We would like to emphasize the following points.

(i) In a previous paper [8], even-parity states of three-valence-electron (nucleon) systems have been found to prefer strongly the coplanar structure. Now this preference is recovered. This arises simply because three-dimensional configurations with better geometric symmetry is prohibited by the QM symmetry; thus this feature originates only from the QM symmetry, but not from dynamics. Hence this finding is expected to be quite general.

(ii) In the plane of the five particles the preference of the axial symmetry has been found. Each pair of spin-parallel electrons remains to be symmetric with respect to a common axis during their motion. Accordingly, the system prefers to form a rectangle (in the $S=0$ and 2 cases) or an isosceles trapezoid (in the $S=1$ case). Strictly speaking, the distribution of the wave function is not well concentrated in the neighborhood of axial-symmetric configurations. However, the motion related to asymmetric distribution is not important and can be neglected.

(iii) Although all the even-parity states prefer the coplanar structures, the S=(even) states and the $S=1$ states prefer different modes of motion. In the S=(even) states the motion is based on the rectangle, i.e., the flattening and prolonging of the rectangle (the R-S-R mode). In the $S=1$ states the motion is based on the isosceles trapezoid, where all electrons rush towards the same end of the axis of symmetry (the planar T2BC mode), then all rush back to the opposite end. The physics underlying these choices is the QM symmetry; this symmetry prohibits the rectangle to appear in the $S=1$ states. Thus, not only the parity but also the permutation symmetry of the spatial part play essential role in determining the structure of quantum states.

(iv) There are two types of nodal surfaces appearing in the multidimensional coordinate space. The first type of nodal surfaces originates from QM symmetry; they are called inherent nodal surfaces [1] because they have to appear at the exact locations in all the states belonging to the same QM symmetry. In fact, they embody the constraint exerted by QM symmetry on the quantum states. The second type originates from dynamics; they depend on the interactions, masses, etc; they are called additional nodal surfaces. Different states may have different numbers of the second type and they may appear at different locations. These two types of nodal surfaces together determine the character and the vigor of internal motion.

Just as what we have found in three-fermion systems [8], all the head states have only, if there is any, the inherent nodal surface. Hence the main feature of the head states is essentially determined by the QM symmetry. Consequently the head states of different systems (atomic, nuclear, etc.), although they may be greatly different in size, mass, strength and range of interaction, etc., may have similar features of structure if they belong to the same QM symmetry [8].

(v) Although only the results of head states are reported, the basic modes found in head states usually appear also as important modes in excited states. This arises because the basic modes are essentially determined by inherent nodal surfaces; these surfaces appear in excited states as well. However, new modes may appear and even become important in excited states.

(vi) We have found two basic modes in even-parity quantum states. Let us investigate their classical correspondence. In the same model (all four electrons are confined on a sphere with radius r_o), the classical set of Lagrange's equations was shown in [1]. Although the general solution of this set is difficult to obtain, it turns out that the following solution:

$$\theta_1=\theta_2=\theta_3=\theta_4=90^\circ\ ,\qquad \phi_1(t)=-\phi_2(t)\ ,\quad \phi_3(t)=-\phi_4(t) \tag{14}$$

with $\phi_1(t)$ and $\phi_3(t)$ satisfying

$$\eta\ddot{\phi}_1=\frac{\sin 2\phi_1}{(1-\cos 2\phi_1)^{3/2}}+\frac{\sin(\phi_1-\phi_3)}{[1-\cos(\phi_1-\phi_3)]^{3/2}}+\frac{\sin(\phi_1+\phi_3)}{[1-\cos(\phi_1+\phi_3)]^{3/2}}\ , \tag{15a}$$

$$\eta\ddot{\phi}_3=\frac{\sin 2\phi_3}{(1-\cos 2\phi_3)^{3/2}}+\frac{\sin(\phi_3-\phi_1)}{[1-\cos(\phi_3-\phi_1)]^{3/2}}+\frac{\sin(\phi_1+\phi_3)}{[1-\cos(\phi_1+\phi_3)]^{3/2}}\ , \tag{15b}$$

where $\eta=2\sqrt{2}mr_0^3/e^2$, is an exact solution of the r-frozen Lagrange equations. When $\phi_1=180^\circ-\phi_3$ is assumed (e_1 and e_3 move in reverse direction), Eqs. (15a) and (15b) are reduced to

$$\sqrt{2}\eta\ddot{\phi}_1=\frac{\cos\phi_1}{\sin^2\phi_1}-\frac{\sin\phi_1}{\cos^2\phi_1}\ . \tag{16}$$

This equation can be integrated; it gives

$$\frac{\eta}{\sqrt{2}}\dot{\phi}_1^2=1/\sin\phi_0+1/\cos\phi_0-1/\sin\phi_1-1/\cos\phi_1\ . \tag{17}$$

It implies a periodic collective oscillation. When $\phi_1=\phi_0$ or $\phi_1=90^\circ-\phi_0$, we have $\dot{\phi}_1=0$; hence the oscillation is from ϕ_0 to $90^\circ-\phi_0$ (ϕ_0 is determined by the initial condition). Evidently, it is an exact periodic oscillation and is

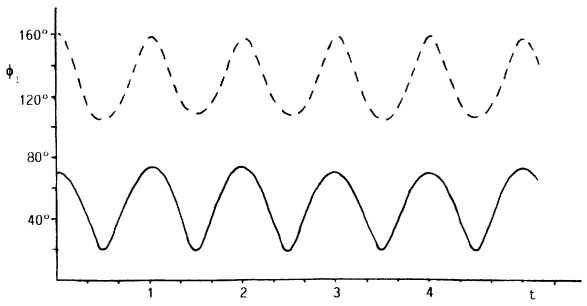

FIG. 9. A typical periodic solution of the classical Lagrange's equations [Eq. (15)]. The solid curve is $\phi_1(t)$, while the dashed curve is $\phi_3(t)$. The initial conditions are $\phi_1=-\phi_2=70°$, $\phi_3=-\phi_4=160°$, and $\phi_i=0$ $(i=1-4)$. The unit of t (abscissa) is the period of oscillation.

just the above R-S-R mode. The period of oscillation is

$$T=2^{3/4}\sqrt{\eta}\int_{\phi_0}^{\pi/2-\phi_0}(1/\sin\phi_0+1/\cos\phi_0 -1/\sin\phi_1-1/\cos\phi_1)^{-1/2}d\phi_1 . \quad (18)$$

Thus the R-S-R mode, just as what we found in [1,9], corresponds to a periodical solution of classical mechanics.

In general Eq. (15) can be solved numerically. When e_1 and e_3 move along the same direction, another type of periodic oscillation can be obtained if the initial condition is properly chosen. A typical example is shown in Fig. 9, which is associated with the planar T2BC mode, where the increase (decrease) of ϕ_1 and ϕ_3 keep in phase.

The existence of basic modes in bound quantum states and the correspondence of these modes with classical periodic solutions are problems gaining research interests [10]. In recent years a semiclassical method based on the path integral [11] has been developed [12] and has been used to explain the energy eigenvalues of the $^1S^e$ helium states [13]. It was found that, among all the contributing classical trajectories, one and only one (asymmetric stretch) gives the dominant contribution to the energy of the lowest intrashell $^1S^e$ helium state of a given Nth shell $(N_1=N_2=N)$. Thus the semiclassical procedure reveals also that the quantum states are intimate to specific modes of classical motion. In this paper the mode of internal motion of a quantum state is essentially defined via the structure of the nodal surfaces; however, alternatively, this motion is expected to also be defined by a semiclassical procedure.

ACKNOWLEDGMENT

This work has been supported by the National Educational Committee of the People's Republic of China.

[1] C. G. Bao, Phys. Rev. A **47**, 1752 (1993).
[2] C. A. Nicolaides, M. Chrysos, and Y. Komninos, Phys. Rev. A **41**, 5244 (1992).
[3] Y. Komninos, M. Chrysos, and C. A. Nicolaides, Phys. Rev. A **38**, 3182 (1988).
[4] K. E. Banyard and R. J. Mobbs, J. Chem. Phys. **75**, 3433 (1981).
[5] R. J. Mobbs and K. E. Banyard, J. Chem. Phys. **78**, 6106 (1983).
[6] C. G. Bao, Z. Phys. D **22**, 557 (1992).
[7] C. G. Bao and T. K. Lim, J. Phys. B **25**, 3245 (1992).
[8] C. G. Bao, Few-Body Sys. **13**, 41 (1992).
[9] C. G. Bao, J. Phys. B **25**, 3725 (1992).
[10] E. J. Heller and S. Tomsovic, Phys. Today **46**, (7), 38 (1993).
[11] R. P. Feynman and H. R. Hibbs, *Quantum Mechanics and Path Integrals* (McGraw-Hill, New York, 1965).
[12] M. C. Gutzwiller, J. Math. Phys. **12**, 343 (1971); *Chaos in Classical and Quantum Mechanics* (Springer, New York, 1990).
[13] G. S. Ezra, K. Richter, G. Tanner, and D. Wintgen, J. Phys. B **24**, L413 (1991).